Contrib Mineral Petrol (1996) 125: 375–392

Dmitri A. Ionov · Suzanne Y. O'Reilly
Yuri S. Genshaft · Maya G. Kopylova

Carbonate-bearing mantle peridotite xenoliths from Spitsbergen: phase relationships, mineral compositions and trace-element residence

Received: 6 October 1995/Accepted: 17 June 1996

Abstract Carbonates of mantle origin have been found in xenoliths from Quaternary basaltic volcanoes in NW Spitsbergen. The carbonates range from dolomite to Mg-bearing calcite and have high Mg-numbers [Mg/(Mg + Fe) = (0.92–0.99)]. In some samples they occur interstitially, e.g. at triple junctions of silicate minerals and appear to be in textural and chemical equilibrium with host lherzolite. Most commonly, however, the carbonates make up fine-grained aggregates together with (Ca,Mg)-rich olivine and (Al,Cr,Ti)-rich clinopyroxene that typically replace spinel, amphibole, and orthopyroxene as well as primary clinopyroxene and olivine. Some lherzolites contain amphibole and apatite that appear to have formed before precipitation of the carbonates. *In situ* analyses by proton microprobe show very high contents of Sr in the clinopyroxene, carbonates and apatite; the apatite is also very rich in LREE, U, Th, Cl, Br. Disseminated amphibole in carbonate-bearing rocks is very poor in Nb and Zr, in contrast to vein amphibole and mica from carbonate-free rocks that are rich in Nb and Zr. Overall, the Spitsbergen xenoliths provide evidence both for the occurrence of primary carbonate in apparent equilibrium with the spinel lherzolites (regardless of the nature of events that emplaced them) and for the formation of carbonate-bearing pockets consistent with metasomatism by carbonate melts. Calcite and amorphous carbonate-rich materials occur in composite carbonate-fluid inclusions, veins and partial melting zones that appear to be related to fluid action in the mantle, heating of the xenoliths during their entrainment in basaltic magma, and to decompression melting of the carbonates. Magnesite is a product of secondary, post-eruption alteration of the xenoliths.

D.A. Ionov (✉) · S.Y. O'Reilly
Key Centre for the Geochemical Evolution and Metallogeny of Continents (GEMOC), School of Earth Sciences, Macquarie University, Sydney, N.S.W. 2109, Australia

Genshaft Yu.S. · Kopylova M.G.
Schmidt Institute of the Physics of the Earth, Gruzinskaya 10, Moscow 123810, Russia

Editorial responsibility: J. Hoefs

Introduction

The occurrence of carbonates and carbonate-rich melts in the upper mantle has been suggested from experimental studies; in particular, carbonate minerals have been shown to be stable in peridotitic assemblages at subsolidus temperatures and upper mantle pressures (Wyllie 1987, and references therein). Recent studies of mantle xenoliths have invoked interaction of carbonate melts with peridotite host rocks to explain the formation and compositional characteristics of some clinopyroxene-rich, apatite-bearing peridotites (O'Reilly and Griffin 1988; Wallace and Green 1988; Ryabchikov et al. 1989; Yaxley et al. 1991; Dautria et al. 1992; Thibault et al. 1992; Hauri et al. 1993; Rudnick et al. 1993). However, carbonates in mantle peridotites have only rarely been reported. Dolomite and magnesian calcite believed to represent quenched carbonate liquids were found in peridotite xenoliths from Spitsbergen (Amundsen 1987) and single xenoliths from the Cape Verde and Canary Islands (Ryabchikov et al. 1989; Kogarko et al. 1995). Carbonates have also been recorded as tiny inclusions in mantle-derived garnet xenocrysts (McGetchin and Besancon 1973; Smith 1987) and diamonds (Bulanova and Pavlova 1987), components of fluid microinclusions (Frezzotti et al. 1994; Schiano et al. 1994) and interstitial glasses (Amundsen 1987) and accessory minerals in some mantle pyroxenites (Wass 1979). Magnesite was found in garnet websterite and eclogite from ultrahigh-pressure metamorphic complexes (Zhang and Liou 1994).

Table 1 Microstructures, mineral assemblages, equilibration temperatures, Mg numbers of olivine and Cr_2O_3 in spinel for peridotite xenoliths from Spitsbergen. Thermometers: *Wells* Wells (1990), *Ca-opx* Brey and Köhler (1990), *Al-Cr-opx* Witt-Eickschen and Seck (1991); all temperatures calculated for 15 kbar pressure. [± present, − absent, *amph* amphibole, *ap* apatite, *dol* dolomite, *maqn* magnesite, *mg-calc* magnesian calcite, *pl* plagioclase, *ol* olivine, *phl* phlogopite, *sulf* sulphide, *spl* spinel, *Al-glass* (Al, Na)-rich silicate glass, *Mg-glass* Mg-rich carbonate-silicate glass, *mg#* Mg number = Mg/(Mg + Fe)]

Sample no.	Location	Microstructure	Exsolution lamellae	Carbonate minerals	Accessory minerals	Al-glass	Mg-glass
4–24–90	Halvdan	Coarse	-	Dol (magn)	-	-	-
4–25–90	”	Coarse-tabular equigr.	Rare (cpx)	Mg-calc, dol	Pl in glass	Rare	Rare
4–36–90	”	Coarse-tabular equigr.	-	Mg-calc, dol	Sulf	Rare	Rare
4–90–9	”	Coarse-tabular equigr.	-	Mg-calcite	Amph	Pockets	+
21–5	”	Coarse-tabular equigr.	-	Mg-calcite	Amph, ap	Pockets	+
21–6	”	Coarse-tabular equigr.	-	Mg-calcite	Amph, ap	Pockets	+
318	”	Coarse-tabular equigr.	Rare	Dolomite	Amph, sulf	-	+
315–6	”	Coarse-mosaic porph.	Kink band	Dol veins	Amph	Rare	Rare
43–86	Sverre	Coarse-mosaic porph.	+	Dolomite	Ap, pl	Pockets	+
39–86	”	Coarse-mosaic porph.	+	Melted, veins	Sulf, amph	Rare	+
63–90–18	”	Coarse-mosaic porph.	+	Dol, calcite	-	Rare	+
25B	”	Coarse to mosaic	Rare	Magnesite	Pl, sulf	-	Recryst
26A	”	Coarse-mosaic porph.	Kink band	Magn veins	-	-	Rare
4A-90–1	Sigurd	Amphibole wehrlite		-	Amph, phl	-	

+ present, − absent, *amph* amphibole, *ap* apatite, *dol* dolomite, *magn* magnesite, *mg-calc* magnesian calcite, *pl* plagioclase, *ol* olivine, *phl* phlogopite, *sulf* sulphide, *spl* spinel, *Al-glass* (Al,Na)-rich silicate glass, *Mg-glass* Mg-rich carbonate-silicate glass, *mg#* Mg number = Mg/(Mg + ΣFe), Cr_2O_3 is in wt.% Thermometers: Wells (1977); Ca-opx = Brey and Köhler (1990); Al-Cr-opx = Witt-Eickschen and Seck (1991); all temperatures calculated for 15 kbar pressure.

In general, the case for mantle carbonates and metasomatism by carbonate melts has been largely based on indirect evidence rather than on studies of natural peridotite xenoliths containing substantial amounts of mantle-derived carbonates.

Amundsen (1987) and Genshaft and Ilupin (1987) have reported spinel peridotite xenoliths from Spitsbergen containing quenched carbonate melts as well as dolomite and magnesite. In a recent publication Ionov et al. (1993) concluded that dolomite in Spitsbergen xenoliths was formed in the upper mantle due to interaction of carbonate melts with wall-rock peridotites and that quenched carbonate melts were due to decomposition of the primary carbonates during the transport of the xenoliths to the surface. Their study focussed on bulk trace-element compositions (determined by solution ICP-MS) of a few carbonate-bearing peridotites and inferences for trace-element characteristics of carbonate-related mantle metasomatism. In this communication, we report results of a detailed petrographic, electron microprobe and proton microprobe study of additional carbonate-bearing peridotite xenoliths from Spitsbergen. The major aims of this work are to describe the range of mineral assemblages in the carbonate-bearing rocks, characterise their phase relationships and mineral compositions (including some trace elements), place constraints on the origin of the carbonates and their host mantle rocks and examine interaction of carbonate melts with mantle peridotites based on natural carbonate-bearing samples.

Analytical methods

Major-element compositions of minerals and glasses were determined with a Cameca Camebax JX 50 electron microprobe at Macquarie University. Standard operating conditions were a 15 kV accelerating voltage with a 20 nA sample current. Mineral analyses were performed using a beam diameter of 2–3 μm; glasses and carbonates were analysed using a defocussed beam (∼ 10 μm). Natural and synthetic oxide and silicate mineral standards were employed for all minerals including carbonates, the data being reduced by the PAP matrix correction procedure (Pouchou and Pichoir 1984). Lane and Dalton (1994) recently demonstrated that microprobe analyses of carbonates assuming stoichiometric oxygen for each analysed element may produce erroneous results using ZAF correction routines, with real to analysed concentration ratios for Ca, Mg, Mn and Fe in dolomite and calcite typically about 1.07. Since the relative errors for the cations in these minerals are very similar their results do not appear to suggest that the accuracy of the Ca:Mg:Fe:Mn ratios may be affected significantly. Carbonate totals calculated from our microprobe analyses (done with the PAP correction) assuming stoichiometric metal/carbon ratios do not yield systematically low values implied for the ZAF correction routines by Lane and Dalton (1994). Analyses reported here are either representative single determinations selected out of a few analyses of a given mineral or averages (when indicated) for phases with homogeneous compositions. No values are reported below detection limits (0.01–0.03 wt.%). Major elements in bulk rocks were determined by X-ray fluorescence spectrometry (XRF) at Macquarie University.

Trace-element analyses in minerals were performed in thin sections by proton microprobe (beam size ∼ 30 microns) using the proton-induced X-ray emission (PIXE) technique at CSIRO, Sydney (Ryan et al. 1990). If three or more single determinations on a mineral yielded very similar results, their spectra were summed and recalculated as a single measurement; this procedure provided lower detection limits and better precision. Otherwise, single representative analyses are given.

Table 1 (continued)

Temperature estimates, core-rim			mg# in ol	Cr_2O_3 in spl
Wells	Ca-opx	Al-Cr-opx		
980–999	1020–999	950–995	0.881	15.9
970	1000–15	1010	0.910	18.4
940	950–965	925–960	0.908	16.5
980	990	975	0.898	14.7
910	915–930	890	0.914	22.0
930	925	910–885	0·912	19.8
900	930–960	900–955	0.915	22.6
860	885–900	960–880	0.904	11.5
920	915	880	0.911	19.4
880	900–910	880–895	0.883	10.0
870	900	945–875	0.901	12.6
910	920	895	0.899	11.3
710–740	1000–790	980–780	0.912	34.7
			0.890	

Sample descriptions

Xenolith occurrences

Abundant mantle and lower crustal xenoliths are found in three Quaternary volcanic centres in NW Spitsbergen: Sverrefjell (Sverre), Halvdanpiggen (Halvdan) and Sigurdfjell (Sigurd). A summary of the geology, tectonic setting and geophysical data for this region has been provided by Amundsen et al. (1987). The xenoliths are contained in nepheline basanitic to hawaiitic lavas; they include "anhydrous" spinel lherzolites and wehrlites, amphibole- and phlogopite-bearing peridotites, garnet and spinel pyroxenites. Here we consider only the carbonate-bearing spinel peridotite xenoliths. Additional information on other xenolith types can be found elsewhere (Furnes et al. 1986; Amundsen et al. 1987; Genshaft et al. 1992).

The carbonate-bearing xenoliths were collected in two volcanic centres: Sverre is a composite basaltic volcano which probably last erupted ca. 100,000 years ago whilst Halvdan is a diatreme ca. 200 m in diameter. The most common peridotite xenoliths at Sverre are 'anhydrous' spinel lherzolites, whereas the Halvdan xenolith suite contains abundant amphibole- and apatite-bearing peridotites. Both carbonate-bearing and carbonate-free peridotite xenoliths were found in both volcanic centres. The majority of the carbonate-bearing samples only contain thin veins of amorphous carbonate-rich material in cracks and along grain boundaries. Xenoliths with unequivocal primary granular carbonates are very rare; those with substantial carbonate contents and largest size (usually 5–10 cm) were selected for this study (Table 1).

Peridotites hosting carbonates

Carbonates were found in "anhydrous" spinel lherzolites and lherzolites containing amphibole and apatite. The carbonate-bearing and carbonate-free xenoliths have similar textures and modal compositions. Spinel lherzolites are coarse- to medium- grained rocks commonly containing 5–12% clinopyroxene (cpx). Clinopyroxene-poor and cpx-rich rocks are subordinate in the peridotite suite. In some samples pyroxenes form clusters or bands and modal compositions may be difficult to estimate precisely in thin sections.

The majority of the spinel lherzolites have two structural groups of minerals. The first group comprises coarse, strained olivine grains (2–4 mm in size) and large orthopyroxene grains (up to 8 mm along the longer axis) which have rounded to irregular grain boundaries. In cpx-rich lherzolites this group also includes large clinopyroxene grains. The second group is made up of fine- to medium-grained, strain-free olivine and pyroxene neoblasts with smooth or straight boundaries and common 120° triple junctions (annealing textures). The microstructures of the peridotites are largely determined by the relative abundances of these two structural groups and range from protogranular (coarse) to mosaic equigranular or porphyroclastic (see Table 1 for a summary). In rocks where the large olivine and pyroxenes predominate (e.g. 26a, 4–36–90) these minerals are usually contiguous and equant; the microstructure is therefore similar to protogranular. In the majority of spinel lherzolites (e.g. 63–90–18, 39–86), the neoblasts are abundant (10–40%) and form mosaic equigranular patches. Sharp contrasts in size and shape between the porphyroclasts and the neoblasts are rare and gradations between the two structural groups are common; few samples have microstructures similar to mosaic porphyroclastic.

Large grains of olivine in almost all xenoliths show kink banding and undulose extinction. These signs of strain are also present, though less common, in large orthopyroxenes; undulose extinction is shown also by some clinopyroxenes. Some of the olivine and orthopyroxene porphyroclasts have subgrains that grade into the neoblasts. Many large grains of pyroxenes have exsolution lamellae in their cores. The orthopyroxenes have very long, fine lamellae (probably high-Ca pyroxene), and euhedral microinclusions of brown spinel; the clinopyroxenes commonly exsolve spinel. In some orthopyroxene porphyroclasts (samples 26a, 315-6), the fine lamellae are bent by several kink planes, with the difference in extinction angles between the opposite ends of the crystals reaching 30–40°. The neoblasts have no exsolution lamellae.

Amphibole-bearing peridotites range from spinel lherzolites that have only rare and small amphibole grains (e.g. 4–90–9) to rocks with 5–8% amphibole (318, 315–6). In samples 21–5 and 21–6 that have moderate amphibole contents (2–5%), some amphibole grains contain resorbed spinel inclusions and appear to have partially replaced spinel. In contrast, samples 318 and 315–6 are rich in both amphibole and spinel; most spinel grains in them are not mantled by amphibole. Amphibole-bearing peridotites generally have more equant minerals and homogeneous grain size than amphibole-free peridotites and commonly have textures transitional between protogranular and mosaic equigranular (21–5, 21–6). Pyroxenes in the amphibole-bearing peridotites usually have no exsolution lamellae except in sample 315–6 which features kinked lamellae in large orthopyroxenes and has microstructure transitional to mosaic porphyroclastic.

Apatite was found in three samples. Of these, two (21–5 and 21–6) contain amphibole and the other (43–86) has no amphibole but contains large pockets of silicate glass. Apatite occurs as single interstitial grains 50–300 μm in size. The grains are anhedral and commonly have rounded and slightly elongated shapes, are of grey colour and have a "speckled" appearance apparently due to the presence of abundant microinclusions (Fig. 1A). Apatite typically does not occur close to amphibole or carbonate, and there is no textural evidence that these minerals and apatite were formed in the same event.

Carbonate segregations

The carbonates are irregularly distributed in the xenoliths and their content is relatively low. Spinel

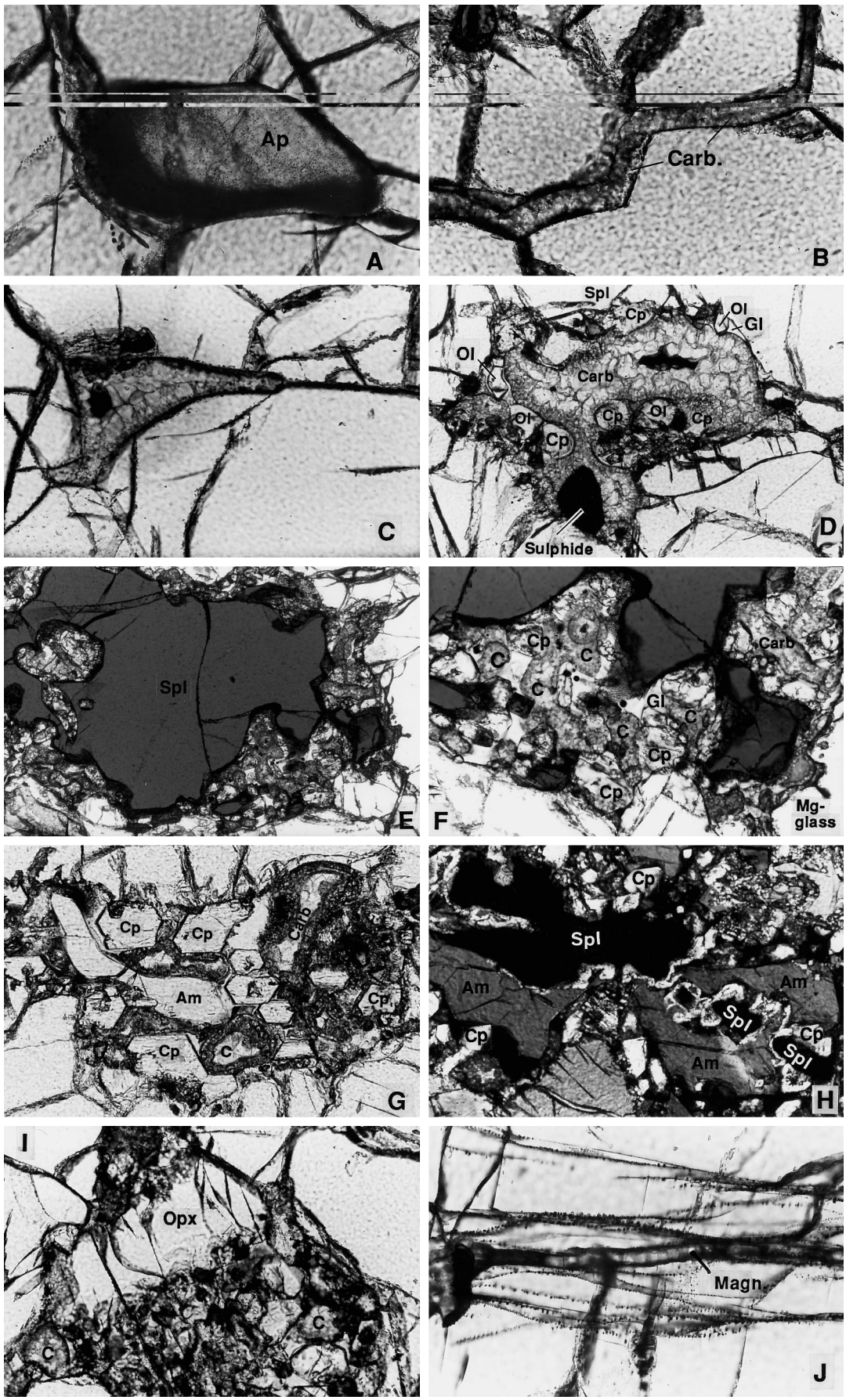
Ap
A
Carb.
B
C
Spl
Cp
Ol
Gl
Carb
Sulphide
D
Spl
E
Cp
C
Carb
Gl
Mg-
glass
F
Am
G
Opx
I
Magn
J
H

Fig. 1A–J

lherzolite 4-36-90 (Table 1) has the most carbonate of the samples reported here with about 2–3%. The carbonates occur as aggregates made up of interlocking grains 20–50 mm in size which form intergranular or cross-cutting veins (Fig. 1B) and small (< 1 mm) interstitial segregations with mosaic textures and sharp curvilinear boundaries (Fig. 1C). Most commonly the carbonates occur within pockets of fine-grained material (Fig. 1D,E) made up of the carbonate aggregates, euhedral or round grains of second generation clinopyroxene and olivine, and occasionally resorbed relict grains of minerals of the host peridotite. In amphibole-free peridotites, the pockets are commonly located at or around spinel (Fig. 1E,F), which has embayed, resorbed outlines and spongy reaction rims where in contact with the carbonate-bearing material. In the amphibole-bearing peridotites, the carbonate-bearing pockets usually surround resorbed amphibole (Fig. 1G); in some cases second generation clinopyroxene forms continuous rims around both amphibole and spinel (Fig. 1H). The clinopyroxene rims around spinel or amphibole and groups of subhedral clinopyroxene grains in the adjacent carbonate-bearing pockets commonly have simultaneous optical extinction (Fig. 1H) and may be parts of large poikilitic crystals.

The carbonates in the fine-grained pockets do not form intergrowths with the silicate or oxide minerals. The carbonates always occur as mosaic aggregates that contain no silicate minerals and have sharp, curved boundaries. Carbonate aggregates within the fine-grained pockets typically have round or smooth curvilinear shapes indicating that they may have crystallised from a liquid carbonate phase. Small pools or thin films of colourless silicate glass exist between some carbonate aggregates and minerals of host peridotite (most commonly at triple junctions; Fig. 1C,D) or more commonly between the carbonate aggregates and euhedral grains of second generation olivine and clinopyroxene with sharp, curved menisci between the carbonate globules and silicate glass (Fig. 1D–G). The content of the silicate glass in unaltered pockets is commonly very low (much lower than that of the carbonate material). Iron-nickel sulphides are common accessory minerals in the carbonate-bearing pockets. They occur either as anhedral or equant grains within the carbonate aggregates (Fig. 1D) or as tiny sulphide drops in the silicate glass (Fig. 1F). In a few samples, the sulphides are abundant and form sulphide-carbonate intergrowths and thin veins.

In many xenoliths minerals of the host peridotite have fine-grained reaction rims or show optical zonation where in contact with the carbonate-bearing pockets. Orthopyroxene usually has very irregular, resorbed margins and thick reaction rims that are composed of fine-grained olivine and clinopyroxene (Fig. 1I). None of the carbonate-bearing pockets contains orthopyroxene relics suggesting that orthopyroxene is the least stable phase in the presence of carbonate. Primary clinopyroxene grains are embayed and strongly zoned in contact with the carbonate and some have overgrowths of euhedral clinopyroxene that have the same optical extinction but different interference colours than the primary clinopyroxene. Some pockets contain small irregularly shaped olivine and clinopyroxene grains that are optically continuous with nearby primary grains of these minerals and appear to be their resorbed relics. The pockets also contain tiny euhedral crystals of second generation spinel. Overall, the carbonate-bearing pockets show reaction relationships with all minerals of the host peridotite, in particular orthopyroxene; the carbonates in the pockets coexist with the second generation clinopyroxene and olivine ($\pm$ spinel).

Many carbonate aggregates are altered. The contact zones of carbonate segregations with the surrounding silicates are usually fine grained and turbid or dark coloured (Fig. 1C–G). They contain small euhedral (hexagonal) magnesite crystals and dark amorphous material replacing the primary carbonates. Most samples also have small patches of brown or colourless silicate glass and amorphous carbonate-rich material. The latter commonly replaces primary carbonates (Fig. 1G) and consists of composite microcrystalline (usually magnesite-ankerite) carbonate spherules immersed in amorphous yellow Mg-rich silicate material which gives low totals when analysed by electron

Fig. 1A–J. Photomicrographs of Spitsbergen xenoliths in plane-polarised (except H) transmitted light. **A** An apatite grain in amphibole-bearing spinel lherzolite 21–5. Note its speckled appearance due to numerous fluid inclusions. Field of view is 0.6 mm. **B** A carbonate vein along grain boundaries in sample 4-36-90, field of view is 0.6 mm. (**C**) A carbonate (Mg-calcite) pocket at a triple junction of olivine grains. A *black spot* in its centre was left by proton microprobe beam. Sample 4–36–90, field of view is 1.2 mm. **D** A carbonate pocket in sample 4–36–90 composed of dolomite and magnesian calcite (see Table 4). Its outer parts enclose grains of secondary olivine (Ol), clinopyroxene (Cp) and spinel (Spl), a large sulphide grain and minor (Na, Al)-rich glass (*Gl*). Fine-grained rims of the carbonate pocket are made up of quenched carbonate melt and secondary magnesite. Field of view is 1.2 mm. **E** Carbonate-bearing pocket replacing a corroded spinel grain. Sample 4-36-90, field of view is 2.5 mm. **F** Same, field of view is 1.2 mm. Note subhedral (Al,Cr-Ti)-rich clinopyroxene crystals, round carbonate (*C*) segregations and interstitial (Na,Al)-rich silicate glass with tiny drops of immiscible sulphide. **G** Relic amphibole (*Am*) in a carbonate-cpx-ol pocket. The clinopyroxene grains are euhedral and have simultaneous extinction; rims of carbonate (*C*) are altered. Sample 21-6, field of view is 1 mm. **H** Clinopyroxene replaces amphibole (*Am*) and spinel, in particular it develops around spinel inclusions in amphibole. Note that both clinopyroxene rimming amphibole and spinel and euhedral clinopyroxene grains in the adjacent carbonate are optically continuous (simultaneous extinction). Sample 21-6, crossed nickols, field of view is 1.2 mm. **I** Replacement of orthopyroxene by an aggregate of carbonate (*C*), clinopyroxene and olivine; Ca content of the secondary pyroxene in the reaction zone is broadly variable (Sample 21-6, Table 3). Field of view 1.2 mm. **J** A series of secondary magnesite veins and arrays of fluid inclusions cross-cutting an orthopyroxene grain. Sample 26A, field of view 0.6 mm

microprobe (Amundsen 1987; Ionov et al. 1993). Tiny, euhedral crystals of magnesite are formed on margin of this material. The textural evidence suggests that the quenched carbonate liquid and amorphous carbonate-rich material were formed as a result of melting and breakdown of primary carbonates (Canil 1990; Ionov et al. 1993). Spinel lherzolite 25B contains abundant interstitial magnesite commonly associated with amorphous or cryptocrystalline secondary material. Sample 25B also has small veins of devitrified brown Fe-Ti-rich glass and plagioclase crystals, but no pockets of second generation olivine and clinopyroxene. Sample 26A has magnesite veins in olivine and orthopyroxene accompanied by arrays of fluid inclusions (Fig. 1J). The textural evidence indicates secondary origin for the magnesite in the xenoliths which may be related to low-temperature processes, e.g. post-eruption alteration of primary carbonates.

Major element composition

Bulk rock major-element compositions were determined for five xenoliths (Table 2). Two duplicate bulk rock samples were prepared from separate pieces of the largest xenolith, 4–36–90. They yielded very similar values indicating sample homogeneity. Four of the xenoliths have moderate contents of Ca, Al, Ti and Na and somewhat high Mg-numbers [Mg/(Mg + Fe) = 0.90–0.91), i.e. they are moderately depleted in "basaltic components" relative to primitive mantle (Hofmann 1988; McDonough 1990). Sample 39–86 has low MgO (38.5%) and high FeO and TiO_2 (8.9% and 0.28% respectively, ie higher than estimates for primitive mantle), with a low Mg-number of 0.885, but has only slightly higher contents of Al, Ca, Na than in the other xenoliths.

The major-element composition of each mineral phase was determined in all carbonate-bearing samples (see Table 3 for representative analyses). The Cr_2O_3 content of spinels is $> 10\%$ and silicate minerals in most samples have Mg-numbers close to or higher than 0.90 (Table 1). The xenolith suite can, therefore, be characterised as slightly to moderately depleted relative to primitive mantle. Olivine in two samples has comparatively low Mg-numbers (~ 0.88), but spinel is not Cr-poor (10–16% Cr_2O_3), indicating that the two rocks apparently were first depleted and then re-fertilised by an Fe,Ti-rich silicate melt. Olivine is poor in CaO (0.04–0.06%) as is usual in spinel peridotites. Amphiboles are pargasites with low K and Ti contents. Pyroxenes have moderate contents of Al, Na and Ti and show at most only minor core-rim zoning. Appreciable zoning is present only at contacts between the primary olivine and clinopyroxene and the carbonate-bearing pockets. The olivine and cpx rims have higher Mg-numbers and Ca contents than the cores and the cpx rims have higher contents of Al, Ti and Cr and lower contents of Na.

Olivine and clinopyroxene within the carbonate-bearing pockets have compositions distinct from those of primary olivine and clinopyroxene (Table 3). Olivine in the pockets has higher Mg-numbers (0.93–0.94) and CaO contents (typically $\geq 0.2\%$) than does primary olivine; the zoned rims of primary olivines show intermediate compositions (e.g. sample 21–6, Table 3). Clinopyroxene in the pockets shows a range of compositions (sample 4–36–90, Table 3), but is typically very rich in Al_2O_3 (up to 10%), Cr_2O_3 (up to 3.5%), TiO_2 (up to 2%), i.e. 2–10 times higher than in the primary clinopyroxene, and has somewhat lower Na_2O contents (below 1%) and higher contents of CaO (up to 24%) than the primary clinopyroxene. Relict cores of the primary clinopyroxene in the carbonate-bearing pockets have the same composition as clinopyroxene outside the pockets whereas the composition of the rims is similar to that of small subhedral clinopyroxene crystals in the pockets (sample 21–6, Table 3). The dramatic change in composition between the cores and rims of the zoned clinopyroxene grains occurs within a few tens of microns and probably results from overgrowth of second generation clinopyroxene on resorbed primary clinopyroxene.

Orthopyroxene shows no zoning in contact with the carbonate-bearing pockets, but has a fine-grained reaction zone (Fig. 1I) composed of pyroxene grains with variable CaO contents (5–19%; sample 21–6, Table 3) and olivine. The former appear to be either

Table 2 Whole rock compositions of selected xenoliths (wt.%); 4–36–90*A* and 4–36–90*B* are duplicate whole rock samples prepared from different parts of xenolith 4–36–90; 4–36–90*av* is the average of the analyses for the duplicates (*ND* not determined)

	43–86	4–36–90A	4–36–90B	4–36–90av	28B	63–90–18	39–86
SiO_2	42.63	42.91	42.51	42.71	44.27	45.03	45.36
TiO_2	0.05	0.06	0.07	0.07	0.06	0.08	0.28
Al_2O_3	2.35	2.30	2.41	2.36	2.27	2.65	3.24
ΣFeO	7.88	7.70	7.68	7.69	8.02	8.01	8.91
MnO	0.13	0.12	0.12	0.12	0.12	0.13	0.14
MgO	44.42	43.01	43.36	43.19	42.60	40.83	38.53
CaO	1.67	2.20	2.36	2.28	1.82	2.36	2.96
Na_2O	N.D.	0.23	0.16	0.20	N.D.	0.25	0.28
K_2O	0.04	0.01	0.01	0.01	0.00	0.00	0.00
P_2O_5	≤ 0.01	0.00	≤ 0.01	≤ 0.01	0.00	0.00	0.00
Total	99.18	98.54	98.69	98.61	99.16	99.34	99.70
mg#	0.909	0.909	0.910	0.909	0.904	0.901	0.885

Table 3 Electron microprobe analyses of silicate and oxide minerals and glasses (wt%) (Ol olivine, *Opx* orthopyroxene, *Cpx* clinopyroxene, Amph amphibole, *Carb* carbonate, *blank entries* below detection limit)

	21–6, primary assemblage							21–6, Carbonate-related assemblage									315–6 Amph
	Ol Core	Opx		Cpx		Spinel Core	Amph Fig. 1F	Cpx relic		Cpx Euhedral	Px's replacing opx Fig. 1I		Ol rim At carb	Olivine In carb	Glasses		
		Core	Rim	Core	Rim			Core	Rim						Mg-rich	Al-rich*	
SiO_2	41.17	56.82	56.66	53.53	53.24		43.83	53.54	48.72	48.44	52.61	54.30	41.40	41.00	52.39	49.82	42.99
TiO_2		0.01	0.01	0.14	0.11	0.11	0.68	0.08	0.82	0.90	0.39	0.17				0.94	1.31
Al_2O_3		2.83	2.52	3.83	3.72	47.17	14.29	3.82	8.48	8.40	4.35	3.69			3.12	22.50	14.48
Cr_2O_3		0.32	0.36	0.74	0.67	19.96	1.38	0.62	1.90	2.00	1.47	0.74		0.07			1.08
ΣFeO	8.53	5.40	5.39	2.12	2.27	10.80	3.33	2.35	2.08	1.88	2.45	4.60	7.30	6.29	11.81	3.87	4.05
MnO	0.14	0.15	0.13	0.02	0.07		0.08	0.04	0.00	0.05	0.09	0.12	0.08	0.11	0.02	0.04	0.05
MgO	49.52	33.78	34.12	16.09	16.26	19.17	18.10	16.27	14.37	14.52	18.16	28.81	50.58	51.37	20.36	3.60	17.55
CaO	0.04	0.56	0.57	21.43	21.66		11.07	21.41	21.69	22.09	19.19	5.78	0.10	0.18	0.47	9.53	11.12
Na_2O		0.03	0.04	1.11	1.04		3.29	1.06	0.91	0.87	0.74	0.36			0.14	7.46	3.63
K_2O							0.63					0.05			0.49	0.20	0.02
Total	99.40	99.90	99.80	99.01	99.04	97.21	96.68	99.19	98.97	99.15	99.45	98.62	99.46	99.02	88.80	97.96	96.28
mg#	0.912	0.918	0.919	0.931	0.927	0.760	0.906	0.925	0.925	0.932	0.930	0.918	0.925	0.936	0.754	0.624	0.885

	21–5, Primary assemblage:					21–5, Carbonate-related				4–36–90, Primary assemblage				4–36–90,Carbonate-related			
	Ol	Opx Core	Cpx Core	Spinel	Amph	Clinopyroxenes		Ol	Mg-rich glass	Olivine	Spinel	Opx	Cpx	Cpx Fig. 1E	Cpx Fig. 1B	Ol Fig. 1B	Mg-rich glass
						Poikilitic	Euhedral										
SiO_2	40.76	56.00	53.09	0.02	43.57	48.60	49.18	41.72	54.67	40.86		55.43	52.30	50.14	46.59	41.32	52.62
TiO_2		0.02	0.13	0.08	0.86	0.95	0.96					0.08	0.24	1.31	2.01		0.20
Al_2O_3		3.01	4.06	48.00	15.00	8.62	8.09		6.57		53.01	3.51	4.59	6.44	9.56		8.57
Cr_2O_3		0.32	0.77	21.45	1.67	2.12	2.75				16.17	0.35	0.68	1.62	2.58	0.06	
ΣFeO	8.41	5.66	2.20	11.02	3.37	2.12	2.26	6.72	7.99	8.92	10.77	5.67	2.36	2.36	2.32	6.87	5.11
MnO	0.13	0.13	0.08		0.08					0.05		0.12	0.08			0.06	
MgO	49.96	34.21	16.13	19.37	17.62	14.49	15.04	51.70	18.30	49.53	19.89	33.65	16.13	15.97	13.89	51.41	13.41
CaO	0.06	0.55	21.80		11.52	22.34	21.84	0.23	0.67	0.06		0.65	21.48	22.26	22.35	0.17	1.82
Na_2O		0.05	1.09		3.46	0.79	0.91		0.31			0.06	1.05	0.56	0.71		0.12
K_2O					0.59				0.72								0.82
Total	99.32	99.94	99.35	99.94	97.74	100.03	101.03	100.37	89.23	99.42	99.84	99.52	98.91	100.66	100.01	99.83	82.67
mg#	0.914	0.915	0.929	0.758	0.903	0.924	0.922	0.932	0.803	0.908	0.767	0.914	0.924	0.923	0.914	0.930	0.824

a fine-grained mixture of phases or metastable phases derived at intermediate stages of the transformation of orthopyroxene through low-Ca clinopyroxene to a (Ca, Al, Cr, Ti)-rich carbonate-related clinopyroxene.

The primary (granular) carbonates are dolomite and magnesian calcite (Table 4). Individual samples may contain both or only one carbonate phase. Only dolomite was found in samples 43–86, 315–6 and 318; only magnesian calcite was found in 21-5, 21-6 and 4–90–9; 4–25–90, 4–36–90 and 63–90–18 contain both, with magnesian calcite being more common. A large number of carbonate grains were analysed in sample 4–36–90 (Table 4). Uniformly distributed dolomite and magnesian calcite were found in the core of the carbonate pocket shown in Fig. 1D. However, no dolomite was found at contacts of that pocket with the primary silicate minerals, and thin veins and small carbonate segregations in that sample are usually made up of magnesian calcite.

Both dolomite and magnesian calcite vary in composition (Table 4). The Ca/(Ca + Mg + Fe + Mn) ratio (X_{Ca}) of dolomite is most commonly within 0.50 ± 0.04 corresponding to a near-ideal dolomite formula $Ca(Mg,Fe,Mn)(CO_3)_2$. However, the X_{Ca} values of Mg-rich carbonate in sample 4–36–90 show what appears to be a continuous range from 0.46 to 0.67 (Table 4) indicating a significant calcite component in some dolomite grains. Two compositional varieties of magnesian calcite were found. The most common one has X_{Ca} of 0.84–0.88; a more Mg-rich magnesian calcite with X_{Ca} of ~ 0.73 coexists with dolomite in sample 63-90-18 (Table 4). The carbonates have high Mg-numbers that are similar to or higher than those in coexisting silicate phases. Manganese is a common minor component of the carbonates. The content of MnO is usually $\leq 0.5\%$, with most common range of 0.2–0.4% MnO. In some dolomite and magnesian calcite grains the content of MnO is significantly higher (1–2.5%) and may be higher than that of FeO (Table 4), as also reported for carbonates from CI chondrites (Endress and Bischoff 1996). The carbonates are poor in sodium, with Na_2O contents usually well below 0.1% and highest Na_2O contents of 0.2–0.4%. No significant core-rim grain zoning was found, but moderate grain-to-grain compositional differences are common in carbonate pockets, e.g. the Mg-number may vary from 0.92 to 1.0 with odd Fe-rich grains (Mg-number ~ 0.8; Table 4, sample 21–6) whilst the content of MnO varies broadly.

Pure calcite occurs in sample 63–18–90 as elongated euhedral crystals in empty or fluid-filled vugs (see also Ionov et al. 1993). Magnesite (Mg-number ~ 0.93) makes up cross-cutting veins in minerals in sample 26A and is abundant in sample 25B. Turbid rims of carbonate pockets show higher contents of Fe and lower contents of Ca and Mg-numbers than primary carbonates (sample 21–5, Table 4). Quenched carbonate glasses have magnesite (Fe-rich) or ankerite compositions (Ionov et al. 1993).

Temperature and pressure estimates

The Wells (1977) two-pyroxene thermometer gives equilibration temperatures ranging from 860 to 980 °C for 13 samples studied (Table 1). The Ca-in-opx (orthopyroxene) method (Brey and Köhler 1990) yields similar or slightly higher T values of 885 to 1020 °C as does the Al-Cr-opx method (Witt-Eickschen and Seck 1991) (880–1010 °C). Sample 26A gives aberrant results with both the Wells thermometer (710–740 °C, core-rim) and the other two thermometers for rims (780–790 °C) which may indicate partial re-equilibration at low temperatures. We also calculated Wells (1977) temperatures for 10 spinel peridotite xenoliths from Spitsbergen from microprobe analyses available in the literature (Furnes et al. 1986; Amundsen et al. 1987). These gave a similar range (900–990 °C) but our data extend to somewhat lower T values. Our T estimates are generally lower than the range of 940–1170 °C obtained by Amundsen et al. (1987) for spinel lherzolites from Spitsbergen using the olivine-opx-spinel thermometer of Sachtleben and Seck (1981). Equilibration pressures cannot be estimated directly but they must be within the stability field of spinel lherzolite (9–18 kbar). The low-pressure limit for the suite (9–10 kbar) is constrained by the upper limit of plagioclase stability in lherzolites at 900–1000° (Green and Hibberson 1970; Jaques and Green 1980) as the xenoliths do not have primary plagioclase (second generation plagioclase occurs in insignificant amounts as phenocrysts in silicate glass veins in few samples) whilst the upper pressure limit is defined by the spinel-garnet transition (O'Neill 1981). A further constraint follows from the requirement that equilibration pressures for the xenoliths should comply with regional geotherm (that should be within the spinel lherzolite stability field for $850\,°C < T < 1020\,°C$); this for example rules out high-P values for the low-T xenoliths. The P-T estimates for garnet pyroxenite xenoliths from Spitsbergen (Amundsen et al. 1987) also suggest that low-pressure values within the estimated P-T range of the spinel lherzolite xenoliths are most likely.

Trace element compositions

Carbonate segregations, apatite, clinopyroxene, amphibole and Mg-rich glass were analysed for trace elements by proton microprobe (Table 5). Carbonates are rich in Sr (1800–3600 ppm). The content of Sr varies within individual carbonate pockets and shows no relation to variation of Fe and Mn. The content of Ba ranges from 130 to 660 ppm, with Sr/Ba ratios ranging from 5 to 18. Carbonates in samples 21–5 and 21–6 yielded high U contents (11–16 ppm) but no Th was detected (detection limit 2–3 ppm). La and Ce contents obtained for carbonate 21–6 (65–110 ppm) are close to

Table 4 Electron microprobe analyses of carbonates and apatite (wt%) (X_{Ca} Ca/(Ca + Mg), *mg#* Mg/(Mg + ∑Fe), see Table 1 for other abbreviations

	4–36–90														4–24–90	26A Fig. 1J Magn	25B Second magn
	Carbonate pocket shown in Fig. 1D (core)								Near rim	Near rim	Rim	Fig. 1F Dol	Fig. 1C Mg-calc	Fig. 1B Mg-calc	Dol		
	Dol	Dol	Dol	Dol	Dol	Mg-calc	Mg-calc	Mg-calc	Mg-calc	Mg-calc	Magn[a]						
ΣFeO		0.30	0.35	0.56	0.50	0.36	0.32	0.54	0.72	0.73	3.11	1.33	0.75	0.75	3.36	5.74	2.53
MnO		0.01						0.34	0.31		0.04		0.31	0.50	0.38	0.11	0.01
MgO	24.17	18.94	17.55	15.10	13.92	6.13	5.04	4.45	5.58	4.74	45.44	18.69	4.36	4.84	13.42	44.02	46.83
CaO	28.28	31.76	37.83	38.29	40.46	47.73	50.27	49.63	51.89	51.02	0.22	34.55	50.97	50.05	35.18	0.37	0.35
Na_2O		0.02				0.05	0.04				0.03	0.05				0.04	
Total	52.45	51.03	55.73	53.95	54.88	54.27	55.67	54.96	58.50	56.49	48.84	54.62	56.39	56.14	52.34	50.28	49.81
mg#	1.000	0.991	0.989	0.980	0.980	0.968	0.966	0.936	0.933	0.920	0.963	0.962	0.912	0.920	0.877	0.932	0.971
X_{Ca}	0.46	0.54	0.61	0.64	0.67	0.84	0.87	0.88	0.86	0.88	0.00	0.56	0.88	0.87	0.62	0.01	0.01

	43–86 Dol	318 Dol	315–6 Dol	63–90–18			21–5				21–6, Transverse across a carbonate pocket					21–6 Mg-calc Fig. 1G	4–90–9 Mg-calc
				Dol	Mg-calc	Calcite	Ap[b]	Mg-calc	Mg-calc	Mg-calc[c]	Mg-calc Rim	Mg-calc	Mg-calc	Mg-calc	Mg-calc Core		
ΣFeO	0.23	4.95	0.44	1.07	1.04		0.37	0.94		2.24	0.77	0.76	0.70	2.70	0.31	2.40	1.01
MnO	0.80	0.30	0.26	1.55	0.91			0.30	2.41	0.33	0.21	0.27	0.38	0.15	0.40	0.23	0.04
MgO	20.72	17.37	19.34	21.88	10.66		0.83	5.35	3.44	7.05	5.28	5.39	6.51	6.16	6.32	5.59	5.63
CaO	30.19	28.79	31.49	32.62	43.57	55.85	53.04	49.68	49.22	46.96	52.73	52.48	51.42	49.77	50.79	50.85	47.87
Na_2O	0.20	0.07	0.42	0.07	0.08		0.42		0.11	0.06	0.05	0.01	0.05	0.06	0.04	0.05	0.04
Total	52.14	51.48	51.95	57.19	56.26	55.85	54.66	56.27	55.18	56.64	59.04	58.91	59.06	58.84	57.86	59.12	54.59
mg#	0.994	0.862	0.987	0.973	0.948	1.00	0.800	0.910	1.00	0.849	0.924	0.927	0.943	0.803	0.973	0.806	0.909
X_{Ca}	0.50	0.50	0.53	0.50	0.73	1.00	0.97	0.86	0.88	0.80	0.87	0.86	0.84	0.82	0.84	0.84	0.85

[a] Secondary magnesite rimming pockets of primary carbonate
[b] Apatite also contains 40.74% P_2O_5, 2.48% Cl and 0.70% F
[c] Turbid grain at silicate glass

their detection limits, and 20 ppm Y was found in a single carbonate grain. In all samples studied, the Sr content in primary clinopyroxene is high (160–310 ppm). In samples 21–5 and 21–6, the carbonate-related clinopyroxene has lower Sr content (110–140 ppm) than does primary clinopyroxene (270–310 ppm), but this is not so in sample 4–36–90. The content of Y is about twice as high in carbonate-related (18–28 ppm) than in primary clinopyroxene (9–13 ppm) whereas the content of Zr is similar in both ranging from 14 to 27 ppm (Fig. 2).

These data may be used to estimate apparent partition coefficients between carbonates and coexisting second generation clinopyroxene ($D_{el\text{-}t}^{carb/cpx}$). Sr strongly partitions into carbonate in the carbonate-bearing pockets, with carbonate/cpx ratios of 17–19 in samples 21–5 and 21–6 where the carbonate is magnesian calcite. The carbonate/cpx ratio for Sr is lower and strongly variable (7–14) in sample 4–36–90 where both

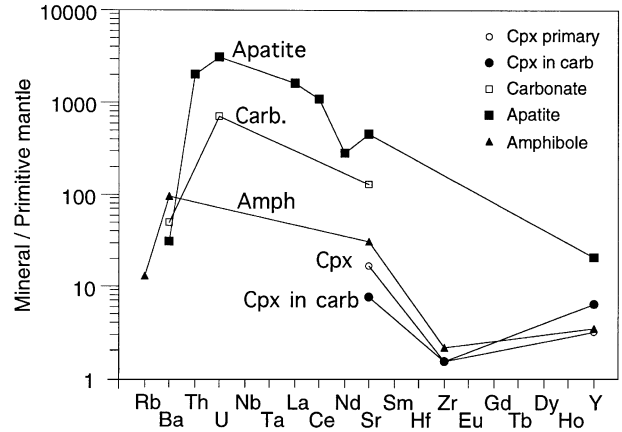

Fig. 2 Trace-element contents of minerals in xenolith 21–5 from proton microprobe data, normalised to primitive mantle estimates (after Hofmann, 1988).

Table 5 Proton probe analyses (in ppm, except Fe in wt% (blank below detection limit)

		Carbonates							Apatites:			Mg-glass 21 − 5
	Detection limits	4–36–90			21–5		21–6		21–5 Av. of 3	21–6 Av. of 4	43–86[a] Av. of 2	
		N-15	N-20	Turbid	Av. of 4	Mn-rich	Av. of 3	Mn-rich				
Fe	0.002%	0.38%	0.59%	3.75%	0.35%	0.14%	0.53%	0.30%	0.25%	0.30%	0.16%	10.6%
Mn	40	1750	3200	1500	1480	11500	1880	12000	560	420	470	80
Ni	5	5		675	19	280		160	8	40	50	4400
Cu	3	≤ 6	≤ 6	67	10	14	7	34	18	20	20	320
Zn	2			10	12	20	8	15	10	7	7	55
Sr	2	3600	1780	1180	2400	3600	2240	2380	8360	6400	8600	80
Ba	40	200	130	135	305	660	400	520	185	150	300	
Y	2			4		≤ 6		20	83	58	59	
La	40						110	65	1000	760	1740	
Ce	50						100		1720	1360	1930	
Nd	100								340	300	570	
Th	2								160	120	160	
U	3				14	16	14	11	61	52	76	
Br	2							74	58			

		Clinopyroxenes									Amphiboles			
		315-6	4–36–90		21–5		21–6				315–6	21–5	21–6	4a–90–1
	Detection limits	Primary Av. of 4	Primary Av. of 2	In carb. Av. of 4	Primary Av. of 2	In carb. Av. of 4	Primary Av. of 6	In carb. Av. of 5	Resorbed relic Core	Rim	Av. of 4	Av. of 4	Av. of 5	Av. of 5
Fe	0.002%	2.02%	2.00%	1.91%	1.81%	1.71%	1.70%	1.62%	1.78%	1.55%	2.72%	2.66%	2.47%	3.48%
Mn	40		670	600	740	680	740	510	860	590		650	620	654
Ni	5	330	350	320	280	310	245	260	260	275	770	716	650	75
Zn	2	20	11	13	12	6	11	8	9	6	11	18	14	20
Rb	2										2	8	7	20
Sr	2	160	240	260	310	140	270	115	280	110	400	650	560	953
Ba	40			160				70			980	890	590	553
Y	2	12	16	28	13	25	9	19	9	18	18	18	14	14
Zr	2	15	27	25	15	15	14	16	18	15	12	25	21	203
Nb	2										< 2	3.5	< 2	161

[a]From Ionov et al. (1993)

magnesian calcite and dolomite are present. This appears to indicate that the $D_{Sr}^{carb/cpx}$ is lower for dolomite than that for magnesian calcite. Alternatively, if our data refer to the equilibrium between clinopyroxene and crystallised carbonate melts they indicate that the $D_{Sr}^{carb.melt/cpx}$ decreases with the Ca content in the melt; this may be the reason why our values for $D_{Sr}^{carb.melt/cpx}$ are higher than those reported by Sweeney et al. (1995) at 46 kbar. Green et al. (1992) determined Sr contents in clinopyroxene and dolomite coexisting with a carbonate melt. Their data indicate a dolomite/cpx partition coefficient of ~ 12, which is of the same order of magnitude as our estimates obtained on natural samples.

The apatite is a chlorine-rich (2.5–3.3 wt.%) variety with high Cl/F ratios (0.1–0.3). It is rich in Sr (6400–8600 ppm), Y (58–83 ppm), Th (120–160 ppm), U (52–76 ppm), Br (58–74 ppm) and light rare earth elements (REE). The La/Nd and La/Y ratios are much higher than chondritic (primitive mantle) values (Hofmann 1988) indicating that the apatites are strongly enriched in light over intermediate and heavy REE. A distinctive feature of amphiboles in the carbonate-bearing samples is their very low contents of Nb (< 3 ppm) and Zr (12–25 ppm). In comparison, amphibole from an amphibole-phlogopite vein in a carbonate-free Spitsbergen xenolith (sample 4a-90-1 from Sigurd) yielded 161 ppm Nb and 203 ppm Zr. Amphibole has the highest contents of Ba (590–980 ppm), Sr (400–650 ppm) and Rb (2–8 ppm) of the silicate minerals in the carbonate-bearing xenoliths. The contents of the lithophile elements in the amorphous yellow Mg-rich silicate material (Mg-glass) are below detection limits except for Sr (80 ppm). Its Ni contents vary strongly and locally are very high, which may result from decomposition of primary Ni-rich sulphides or olivine.

Discussion

Primary nature of carbonate and effects of secondary alteration

We consider that the following lines of textural and mineralogical evidence point to a primary origin for the carbonate (dolomite and magnesian calcite) in the Spitsbergen xenoliths. We emphasise that we call the carbonate "primary" in the sense that it was present in the mantle rocks before their subsequent entrainment in basaltic magma regardless of textural relationships of carbonate with host peridotite (see also Ionov et al., 1993).

1. Common association of carbonate with second generation olivine and clinopyroxene that have distinctive morphologies and chemical compositions inconsistent with derivation either from host basaltic magma or by post-eruption alteration.
2. The preservation of pristine silicate glass and sharp, curved boundaries of carbonate aggregates in carbonate-bearing pockets. Both alkali silicate glasses and magmatic carbonates are easily altered in the presence of CO_2-rich, percolating pore water (Macdonald et al. 1993).
3. The carbonate compositions generally match those obtained experimentally for carbonates coexisting with peridotites in the *P-T* stability field of spinel lherzolites (Dalton and Wood 1993b) and with the compositions of some igneous carbonates (Macdonald et al. 1993).

Textural and chemical evidence suggests that in many xenoliths carbonate has been partially altered both during ascent in the host magma and at the surface. Quenched carbonate liquid and amorphous carbonate-rich materials were formed as a result of decompression melting and breakdown of primary carbonates (Wyllie et al. 1983; Canil 1990; Ionov et al. 1993). The Mg-rich glass may have been formed by decompression-induced dissolution of olivine into a pre-existing carbonate-rich melt. Textural evidence indicates a secondary origin for magnesite in the xenoliths, most probably related to low-temperature processes. Fine-grained magnesite that commonly occurs in the rims of carbonate aggregates and in pools of the Mg-glass may have been formed due to post-eruption re-equilibration and alteration of primary carbonates and their breakdown products. Cross-cutting magnesite veins and interstitial magnesite in samples 25B and 26A appear to have been formed by alteration of the xenoliths by circulating CO_2-rich water (Frost 1985). Fresh samples that preserved the original textures and compositions form the basis of the following discussion.

Pre-carbonate history of Spitsbergen mantle peridotites

Textural data suggest that the formation of the carbonate aggregates and related fine-grained pockets was the latest significant event that affected Spitsbergen peridotites in the mantle and to properly assess its effects it is important to identify and characterise preceding events. Major-element compositions of the peridotite xenoliths and their minerals indicate that the xenolith source experienced moderate depletion in "basaltic components" probably as a result of extraction of partial melts. Ubiquitous signs of strain in porphyroclasts indicate subsequent deformation that might be related both to the location of the xenolith occurrences close (150 km away) to a spreading centre and transform fault zone and to regional lithospheric thinning (Amundsen et al. 1987). The presence of the two structural groups of minerals (porphyroclasts and neoblasts) and of exsolution phenomena in pyroxenes suggest that the deformation was followed by partial annealing and unmixing of pyroxene solid solutions during the cooling of the peridotites.

There is no textural or chemical evidence that would indicate precipitation of carbonate and amphibole or apatite in the Spitsbergen rocks during a single event. Amphibole occurs both in carbonate-bearing and carbonate-free peridotites. The equant microstructures and limited mineral deformation in the amphibole-bearing peridotites indicate that amphibole formation may have been accompanied by re-crystallisation. In the carbonate-bearing rocks amphibole breakdown contributed to the formation of the carbonate-bearing pockets. Textural evidence suggests that amphibole was formed in metasomatic events preceding formation of the carbonate aggregates. Dautria et al. (1992) described a similar situation for xenoliths from the Sahara in which the first metasomatic event precipitated phlogopite and the later event involved interaction with a carbonate melt. Apatite typically does not occur close to carbonate or amphibole in the Spitsbergen samples and its grains are larger than are minerals in carbonate-bearing pockets (Fig. 1A). Formation of apatite must have preceded carbonate formation and may not have been directly related to precipitation of amphibole.

Trace-element composition of primary clinopyroxene in the Spitsbergen xenoliths does not appear to have been affected by the presence of carbonates. The contents of Sr in the primary clinopyroxene (160–310 ppm) are much higher than in clinopyroxene from fertile or moderately depleted lherzolites that have experienced no metasomatic enrichment (20–80 ppm) (Galer and O'Nions 1989; Ionov et al. 1995a). The clinopyroxene is Sr-rich both in amphibole- and apatite-bearing lherzolites as well as in sample 4–36–90 (240 ppm Sr) that has neither amphibole nor apatite. This suggests that some Spitsbergen peridotites underwent cryptic metasomatism that may not have been a result of the same metasomatic events that precipitated amphibole and apatite. The content of Sr in the primary clinopyroxene does not show core-rim zoning or significant grain-to-grain variation. This evidence for equilibrated Sr enrichment contrasts with the extreme textural and major element differences between the primary clinopyroxene and that in carbonate-bearing pockets. In two out of three analysed samples the primary clinopyroxene contains much more Sr than does the carbonate-related clinopyroxene, and the Sr contents are similar in the primary and carbonate-related clinopyroxene for the third one (Table 5). It appears therefore that the high Sr in primary clinopyroxene is not directly related to the presence of carbonates in the rocks. It may be possible however that the Sr enrichment occurred at an early stage of a long-term event that later resulted in the formation of carbonate-bearing pockets.

Comparison with experimentally determined carbonate stability and compositions

Numerous experimental studies have defined the stability of carbonates in the model system CaO–MgO–SiO_2–CO_2 under mantle pressure and temperature conditions (e.g. Brey et al. 1983; Wyllie et al., 1983). Recently Dalton and Wood (1993b) investigated the effect of Fe on carbonate stability in lherzolite assemblages and reviewed data constraining subsolidus reactions that limit carbonate stabilities in natural lherzolite containing Fo_{90} olivine (Fig. 3). In the temperature range 860–1020 °C (i.e. the range calculated for Spitsbergen xenoliths reported here), magnesite is stable in lherzolites at pressures above 25–32 kbar followed by dolomite and magnesian calcite as pressure decreases. The reaction which separates the fields of dolomite and magnesian calcite is (Dalton and Wood 1993b) (Fig. 3):

$$2CaCO_3 + 2MgSiO_3 = CaMg(CO_3)_2 + CaMgSi_2O_6 \quad (1)$$

calcite opx dolomite cpx

At pressures below 10–16 kbar in the T range of 860–1020°C carbonates become unstable in lherzolite assemblages due to the reaction (Wyllie et al. 1983; Dalton and Wood 1993b) (Fig. 3):

$$CaCO_3 + MgCO_3 + MgSiO_3 = CaMgSi_2O_6 + Mg_2SiO_4 + CO_2 \quad (2)$$

carbonate solution opx cpx ol fluid

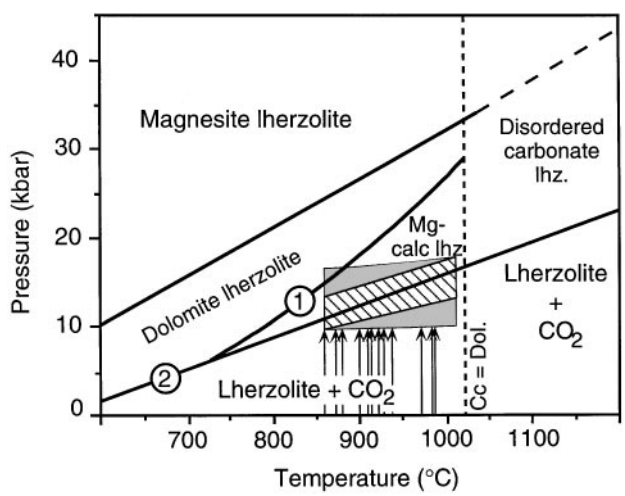

Fig. 3. Location of subsolidus equilibria in lherzolitic compositions in the system CaO–MgO–FeO–SiO_2–CO_2 with Fo_{90} taken from Dalton and Wood (1993b). Carbonate is unstable below reaction (2); reaction (1) separates stability regions of dolomite (dol) and magnesian calcite (*Mg-calc*, *Cc*). *Shadowed box* shows *P-T* stability field for the Spitsbergen carbonate-bearing xenoliths based on calculated equilibration temperatures using two-pyroxene (Wells 1977) and Ca-opx (Brey and Köhler 1990) thermometers and a pressure range defined by the low-*P* (Green and Hibberson 1970) and high-*P* (O'Neill 1981) stability limits for spinel lherzolite with Mg-number of 0.9 and X_{Cr}^{Spl} of 0.1. *Hatched field* shows a *P-T* range for the Spitsbergen lherzolite xenoliths taking into account possible shapes of geothermal gradients for areas of alkali basaltic volcanism. *Arrows* show *T* estimates (Wells 1977) for individual spinel lherzolite xenoliths. *P-T* estimates for garnet pyroxenite xenoliths from Spitsbergen (Amundsen et al. 1987) obtained using thermometer of Wells (1977) and barometer of Nickel and Green (1985) plot slightly below reaction (2)

These reactions as shown on Fig. 3 were calculated for the CMFS-CO_2 system (Dalton and Wood 1993b) and addition of other components of mantle lherzolites (Al, Cr, Ti, Na) that preferentially reside in clinopyroxene may favour clinopyroxene stability and would perhaps shift the positions of these reactions slightly, e.g. to enhance dolomite stability in reaction (1). The estimated *P-T* field for the Spitsbergen xenolith suite overlaps the reaction boundary (2) indicating that carbonate (magnesian calcite) may be stable at least in some of the xenoliths. It is not likely however that any of the xenoliths have equilibrated at pressures as high as 15–16 kbar required for dolomite stability at 850–900 °C since that would imply an unusually low heat flow for an area of alkali basaltic volcanism (Jones et al. 1983; Amundsen et al. 1987). The occurrence of magnesite in some Spitsbergen xenoliths (see also Amundsen (1987), Genshaft and Ilupin, 1987) cannot be explained by experimental data and must be related to alteration processes consistent with textural evidence.

Experimental evidence indicates that carbonates in mantle peridotites must have similar or slightly higher Mg-numbers than those of coexisting olivine and pyroxenes (Brey and Green 1976; Ryabchikov et al. 1989; Dalton and Wood 1993b). Carbonate compositions at the calcite-dolomite join in the system $CaCO_3$–$MgCO_3$ at $T < 1050$ °C (below the solvus crest) show broad, temperature-dependent variation of the magnesian component in the calcite solid solution (Irving and Wyllie 1975). In peridotite systems, dolomite with X_{Ca} of 0.5–0.6 and magnesian calcite with X_{Ca} up to 0.77 were observed in Fe-bearing experiments at 20 kbar/1000–1050°C (Dalton and Wood 1993b); magnesian calcite with X_{Ca} of 0.68–0.74 was produced in the Fe-free system at 15 kbar/950–975 °C (Wyllie et al. 1983).

The most common carbonate phase in the Spitsbergen xenoliths appears to be magnesian calcite (X_{Ca} 0.84–0.88), which occurs in most of the xenoliths studied and is either the only or the most abundant carbonate mineral in the samples rich in carbonates (4–25–90, 4–36–90, 21–5, 21–6). Overall, the carbonate compositions range from dolomites (X_{Ca} commonly 0.46–0.54, in some samples up to 0.67) to Mg-calcites with low contents of the $MgCO_3$ component, not unlike those produced experimentally. The most calcic dolomite ($X_{Ca} = 0.67$; sa. 4–36–90) and most magnesian calcite ($X_{Ca} = 0.73$; sa. 63–90–18) have quite similar X_{Ca} thus, the analyses span a rather large section of the calcite-dolomite solid solution though it is not clear if all of them show equilibrated compositions. For instance, both dolomite and magnesian calcite were produced in some experiments of Dalton and Wood (1993b) at 20 kbar/1000–1050 °C, but Dalton and Wood concluded that only magnesian calcite is the stable carbonate in the peridotitic assemblage as the dolomite does not occur in contact with clinopyroxene whereas the magnesian calcite does. This may also be the case for xenolith 4–36–90 in which dolomite and magnesian calcite coexist inside large carbonate pockets, but in which only magnesian calcite was found at contacts of the pockets with the host lherzolite. The Mg-numbers of magnesian calcite in sample 4–36–90 (0.93 ± 0.02, see Table 4) are similar to Mg-numbers of olivine in the carbonate pockets but lower than the Mg-number of coexisting dolomite (0.98). Dolomite has higher Mg-numbers than does magnesian calcite also in samples 63–90–18 (Table 4) and 4–25–90. This is consistent with experimental results (Dalton and Wood 1993b) indicating that addition of Ca to dolomite decreases the Mg-number of the carbonate in equilibrium with Fo_{90} olivine.

The *P-T* estimates and experimental data indicate that dolomites are not likely to be equilibrium phases in the Spitsbergen spinel lherzolite xenoliths but that magnesian calcites might be. Interstitial carbonate material and small pockets made up of magnesian calcite that show no or limited reaction relationships with minerals of the host peridotite (Fig. 1B,C) may represent carbonates that are in equilibrium with the lherzolites (regardless of the nature of events that emplaced them). Such interpretation is not inconsistent with the presence of small-scale reaction zones between the carbonates and the host lherzolite (e.g. Fig. 1D) as these may result from re-adjustment of pre-existing carbonates to changing *P-T* conditions or from interaction of injected carbonate melt with host lherzolite to produce equilibrium carbonate compositions (Dalton and Wood 1993a).

Formation of carbonate-bearing pockets by reaction of carbonate melt with peridotites

Textural position of carbonates in the Spitsbergen xenoliths suggests that the carbonates were formed from carbonate-rich melts that intruded mantle peridotites since the carbonates most commonly form cross-cutting veins or occur within pockets that replace primary minerals of the peridotites. The shapes of some interstitial carbonate segregations (Fig. 1C) closely resemble those of interconnected pools of a dolomitic melt in an olivine matrix observed in melting experiments (Hunter and McKenzie 1989). The carbonate-bearing pockets could not have been produced by reaction of a CO_2 fluid with lherzolites in the carbonate stability field [at higher pressures than reaction (2)] because such a process would consume clinopyroxene and olivine to produce orthopyroxene and carbonate, which is contrary to the textural evidence. Carbonate melts are not stable in the *P-T* field of the Spitsbergen xenoliths (Fig. 4). The melts must have been hotter than the peridotites they invaded and either quenched or heated the wall-rocks, reacted with them and then froze up. The lack of significant major element zoning in

primary minerals of the xenoliths indicates that any heating related to carbonate melt percolation must have been local and short lived.

The only silicate minerals consistently stable with carbonate in the reaction pockets are fine-grained clinopyroxene and olivine that differ in composition from the coarse olivine and clinopyroxene that occur outside the carbonate-bearing pockets (Table 3). The carbonate-related clinopyroxene has higher contents of Al, Ti and Cr than does clinopyroxene in the primary assemblage. Elements Ti and Cr have contrasting behaviour in the pyroxene/silicate melt system during partial melting or crystallisation and their simultaneous enrichment in clinopyroxene crystallising from a silicate melt would be unlikely. High Ca contents and Mg-numbers of the second generation olivine also indicate an origin from a carbonate rather than silicate melt (Dalton and Wood 1993a). Both the chemical data and textural evidence (e.g. formation of poikilitic cpx crystals, Fig. 1H) suggest that the (Al,Cr,Ti)-rich clinopyroxene, the (Ca,Mg)-rich olivine and associated carbonates formed as a result of metasomatic interaction of carbonate-rich melts with the host peridotite. Small pools of (Na,Al)-rich silicate glass occurring between the carbonate globules and second generation olivine and clinopyroxene (Fig. 1F) suggest that a silicate liquid may have been formed in this process. The lack of textural and chemical equilibration between the host peridotites and the carbonate-bearing pockets indicates that the formation of the pockets took place shortly before the xenoliths were brought up to the surface.

The carbonates in Spitsbergen xenoliths appear to be in local equilibrium with the fine-grained olivine and clinopyroxene in the carbonate-bearing pockets [*cpx* + *ol* + *carbonate* is a stable assemblage also at pressures below the decarbonation reaction (2)], but may be disequilibrium phases relative to the primary lherzolitic (i.e. opx-bearing) assemblage in some samples. This situation is consistent with the position of a large part of the estimated xenolith *P-T* field outside the carbonate stability field (Fig. 3). Such an interpretation implies, therefore, that the carbonates in some of the Spitsbergen xenoliths may be metastable phases produced by quenching of residual batches of carbonate melts that locally survived reaction with orthopyroxene, e.g. because they were "jacketed" by reaction products. The carbonate melt invasion appears to be a very recent event immediately preceding eruption of host basalts. Given sufficient time, the carbonates would have reacted out completely to form either aggregates of clinopyroxene, olivine and residual spinel or clinopyroxene rims around orthopyroxene. Parageneses like these have been found in peridotite xenoliths from many localities worldwide and attributed to carbonate metasomatism (Yaxley et al. 1991; Hauri et al. 1993; Rudnick et al. 1993; Ionov et al. 1995b). The unusual (Al,Cr,Ti)-rich clinopyroxenes apparently are stable only in equilibrium with carbonate melt, and after the disappearance of carbonates the pockets would re-crystallise to produce aggregates of diopside, spinel and probably amphibole or feldspar similar to those found in xenoliths from Algeria (Dautria et al. 1992). One can speculate that at high temperatures the interaction of carbonate melt with peridotite could induce partial melting of host peridotite and give rise to "melt pockets" consisting of olivine and clinopyroxene "phenocrysts" in a silicate glass with (originally CO_2-filled) voids (Hauri et al. 1993; Ionov et al. 1993, 1994). Such a mechanism in particular would explain

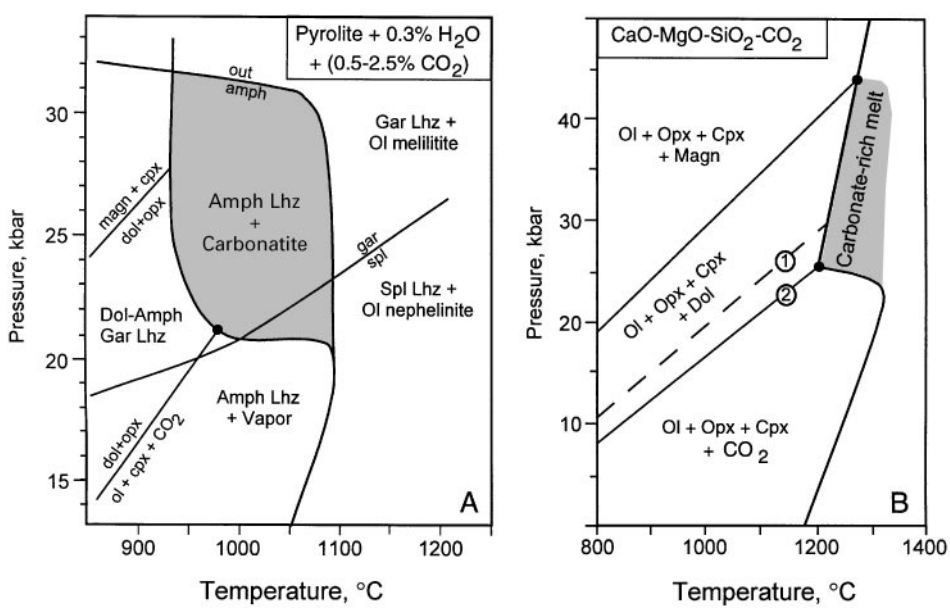

Fig. 4A, B Location of the solidus and of subsolidus equilibria in CO_2-bearing lherzolitic compositions: **A** an amphibole-rich Hawaiian pyrolite (Wallace and Green 1988), **B** the system CaO–MgO–SiO_2–CO_2 (Dalton and Wood 1993b). *Shadowed areas* show fields of carbonate-rich melts. Reactions (1) and (2) same as in Fig. 3. (*Lhz* lherzolite, *dol* dolomite, *magn* magnesite, *amph* amphibole, *ol* olivine, *opx* orthopyroxene, *cpx* clinopyroxene, *gar* garnet, *spl* spinel).

high Mg-numbers of olivine and cpx cores (recording equilibration with a carbonate melt) that contrast with the low Mg-numbers in the host silicate glass.

The appearence of carbonate in reaction pockets implies disequilibrium between carbonate melt and peridotite and the seemingly obvious place for the reaction is at pressures below reaction (2). It cannot be ruled out, however, that the reaction of initial carbonate melt with host lherzolites produced carbonate minerals that were in equilibrium with lherzolite and therefore could take place at pressures above decarbonation reaction (2). The xenolith *P-T* box in Fig. 3 spans reaction (2) and would appear to support both possibilities. The latter scenario could be possible if the parental carbonate melt was derived from source rocks with a composition different from those of Spitsbergen xenoliths (e.g. from fertile lherzolites, (Wallace and Green 1988) or if it was generated at *P-T* conditions above the xenolith box in Fig. 3, intersected the solidus ledge as it moved upwards and cooled back into the carbonate field (Fig. 4). Important factors in such a scenario would be as follows:

1. Melt temperature: the lack of orthopyroxene and very unusual clinopyroxene compositions in the carbonate-bearing pockets does not allow reliable temperature estimates, but it is most likely that intruding carbonate melts were hotter than wall-rock peridotites, at *P-T* conditions beyond the stability field of carbonates in lherzolite. Carbonate melts that rise up adiabatically from their source regions (Fig. 4) to the depth range of the Spitsbergen xenoliths (9–18 kbar, Fig. 3) would originally be on the high-*T* side of the decarbonation reaction (2) and react with host rock, but subsequent cooling to the ambient $T \leq 1000\,^{\circ}C$ could bring the melt/peridotite system to the magnesian calcite stability field and the residual melt should quench without reacting out.
2. Melt composition: experimental work of Dalton and Wood (1993a) has shown that near-solidus carbonate melts in equilibrium with mantle lherzolites become more Ca-rich at lower pressures and that equilibrium melt compositions are different for depleted and fertile peridotites. Upwards transport of a primary dolomitic carbonate melt would result in its interaction with wall-rock lherzolites to produce more Ca-rich compositions in the carbonate stability field [i.e. on the low-*T*, high-*P* side of the reaction (2)]. Similarly, melts derived from a fertile source would react with depleted peridotites at the same *P-T* conditions. The presence of metastable dolomite in the Spitsbergen xenoliths can probably be explained by intrusion of a dolomitic melt, with rapid crystallisation of small batches of the initial melt as interstitial dolomite (except in direct contact with orthopyroxene). Incomplete reaction of larger melt batches with host lherzolite could produce equilibrium magnesian calcite at the contacts of carbonate aggregates and dolomite/Mg-calcite mixtures in their cores. The dolomite could only have been preserved in the xenoliths if they were brought up to the surface shortly after its formation because dolomite would eventually be replaced by magnesian calcite through subsolidus diffusion.
3. The presence of (Al,Cr,Ti)-rich minerals: current experimental data indicate that Al, Cr and Ti have low solubilities in carbonate melts (Dalton and Wood 1993a). Elevated contents of these elements in lherzolite may favour clinopyroxene stability in decarbonation reaction (2) because clinopyroxene can accommodate much more of these elements than can orthopyroxene or carbonate melt. Thus the reaction boundary in natural peridotites might shift to higher pressures than those shown in Fig. 3. This shift may be the reason that many of the carbonate-bearing pockets develop around the (Al,Cr,Ti)-rich phases spinel and amphibole. In other words, the (Al,Cr,Ti)-enrichment in the clinopyroxenes associated with carbonate pockets could be explained by preferential reaction of carbonate melt with spinel and amphibole (that have lowest melting points among the peridotite minerals, Olafsson and Eggler 1983) to liberate these elements for the newly forming clinopyroxene and facilitate carbonate reaction with orthopyroxene.

Carbonate melt compositions

It is unlikely that the initial carbonate-rich melts have been produced by devolatilisation of the basaltic magma that brought up the Spitsbergen xenoliths to the surface. Experimental evidence has shown that carbonate melts in equilibrium with lherzolite can be produced only above the point where reaction (2) intersects the solidus and dolomite is a solidus phase (Fig. 4), i.e. at higher pressures than the *P-T* range for the xenoliths (J. Dalton, personal communication, 1995). The initial carbonate-rich melts may have been derived by partial melting of carbonate-bearing peridotite mantle at deeper levels. Here we use the term "carbonate melt", consistent with the distinction between carbonate and carbonatitic liquids made by Dalton and Wood (1993a) and Ionov et al. (1993). The term carbonatite liquids should be reserved for those melts which are compositionally close in terms of major and trace elements to carbonatite rocks. Carbonate melts that are generated in the mantle, and may be parental to such rocks, may have quite distinct compositions.

Dalton and Wood (1993a) have shown that the first melts from a carbonated, depleted lherzolite at pressures > 25 kbar are carbonate with $Ca/(Ca + Mg)$ ratios of 0.72–0.74 and that primary carbonate melts from fertile mantle are more sodic with $Ca/(Ca + Mg + Fe + Na)$ of 0.52 and $Na/(Na + Ca + Mg + Fe)$ up to 0.15. The equilibrium melt becomes more calcic with decreasing pressure consistent with earlier experimental evidence for the shift of the temperature minimum for the solidus and liquidus curves in the

$MgCO_3$–$CaCO_3$ system to higher Ca/(Ca + Mg) ratios with decreasing pressure (Irving and Wyllie 1975). Dalton and Wood (1993a) suggested that calcio-carbonatites, by far the most important carbonatites at the Earth's surface, can be generated through reaction of these melts with harzburgitic or lherzolitic assemblages at low pressures provided that the melts contain small amounts of water or other fluids to depress their solidi. A consequence of reaction with carbonate melt is to transform the bulk composition of the peridotite from that of harzburgite or lherzolite to wehrlite. This concept is generally consistent with the textural and chemical evidence from the Spitsbergen xenoliths reported here. The reaction of carbonate melt with lherzolites observed in the Spitsbergen xenoliths has produced wehrlitic compositions only locally, in fine-grained pockets, probably because the amount of melt was not sufficient or because the initial melt did not contain enough fluids to suppress its solidus and quenched before the reaction was complete.

The X_{Ca} of the initial carbonate melt can be estimated based on the observation of Dalton and Wood 1993a) that the Ca content of olivine coexisting with a carbonate melt is proportional to the Ca/(Ca + Mg + Fe + Na) ratio of the melt. The CaO content in olivines from carbonate-bearing pockets (0.16–0.24%) indicates that they may have coexisted with a dolomitic melt of Ca/(Ca + Mg + Fe + Na) ratio about 0.65. A consequence of the reaction between orthopyroxene and Mg-rich carbonate melt at low pressures to produce olivine and clinopyroxene is that the melt becomes more calcic, e.g. experiments at 15 kbar produced carbonate melt with the Ca/(Ca + Mg) ratio of 0.88 (Dalton and Wood 1993a). The common occurrence of magnesian calcite with very similar compositions in the Spitsbergen xenoliths would be consistent with the origin of carbonates as residues from such a reaction. Magnesiam calcite ($\sim$ 10% $MgCO_3$) was also produced in experiments (20 kbar/1000°C) by interaction of alkali-rich dolomitic melt with wehrlite (Thibault et al. 1992). Immiscible magmatic carbonates with compositions similar to those of magnesian calcites from Spitsbergen xenoliths were reported in a harzburgite xenolith from Canary Islands (X_{Ca} 0.84–0.92, Mg-number $\sim$ 0.95, Kogarko et al. 1995) and in ash flow tuffs in Kenya (X_{Ca} 0.86–0.90, Mg-number $\sim$ 0.97, Macdonald et al. 1993).

Rapid crystallisation and incomplete reaction of the initial Mg-rich carbonate melt in colder lherzolites may produce carbonates with a range of Ca/(Ca + Mg) ratios. Experimental results in the binary $MgCO_3$–$CaCO_3$ system (Irving and Wyllie 1975) have shown that the temperature minimum on the liquidus and solidus shifts from a composition with a Ca/(Ca + Mg) ratio of 0.58 at 30 kbar to that of $\sim$ 0.7 at 15 kbar and $\sim$ 0.8 at 12 kbar. This means that melting temperature of a carbonate melt will increase if its Ca/(Ca + Mg) ratio changes from the low melting T value at a given pressure and may increase with a lower P at a given Ca/(Ca + Mg) ratio. If these results can directly be applied to multi-component carbonate compositions in natural peridotite systems it would follow that the increase in the Ca content of a melt may cause it to crystallise before the reaction with host peridotite produces an equilibrium melt composition.

Based on experimental results (Dalton and Wood 1993a) it can be suggested that the parental carbonate melt was derived from a depleted peridotite source. The Spitsbergen carbonates are very poor in sodium and there is no evidence for Na-enrichment in the carbonate-bearing pockets. Also the jadeite component of the second generation clinopyroxene is low (with 0.7–0.9 wt.% Na_2O as compared to $> 1\%$ Na_2O in first generation clinopyroxene). A Na-rich carbonate melt would tend to buffer this component to higher concentrations as suggested by Yaxley et al. (1991). Alternatively, one can speculate that some Na escaped with CO_2-rich fluids produced by reaction of carbonate melt with peridotite or that residual Na in the carbonate was subsequently leached by ground water during post-eruption alteration.

Concluding remarks

We have shown that primary (in the sense that they were present in mantle peridotites before their entrainment in basaltic magma) carbonates, dolomite and magnesian calcite occur in some lherzolite xenoliths from Spitsbergen. The carbonates precipitated from carbonate melts that intruded the lherzolites shortly before their transport to the surface as xenoliths. Reaction of the initial Ca–Mg carbonate melts with host lherzolites produced a range of carbonate mineral compositions and fine-grained pockets with wehrlitic assemblages, consistent with experimental evidence. Magnesian calcites with X_{Ca} of $\sim$ 0.88 may be equilibrium phases in the wehrlite pockets and some spinel lherzolites in the uppermost mantle beneath Spitsbergen. Alternatively, patches of second generation olivine and clinopyroxene in vesicular silicate glass that occur in some xenoliths may be related to breakdown of carbonate. Apatite and amphibole as well as Sr-rich clinopyroxene were formed in some of the Spitsbergen xenoliths prior to the intrusion of the carbonate melts, which precipitated no volatile-bearing minerals. The absence or presence of apatite or amphibole (Green and Wallace 1988; Yaxley et al. 1991) therefore may not be relevant as indicators of carbonate-related metasomatism. Accessory Fe–Ni sulphides are common in the carbonate and may be a typical component of the carbonate-rich melts (e.g. as immiscible sulphide liquid Kogarko et al. 1995).

The ubiquitous lack of carbonates in mantle xenoliths from alkali basalts seems to be consistent with their instability at the prevailing P-T conditions of

mantle spinel and garnet-spinel peridotites in the areas of alkali basaltic volcanism because of the position of their elevated geotherms close to the decarbonation reaction. If this is the case for the uppermost mantle beneath Spitsbergen, as seems to be indicated by *P-T* estimates on garnet-bearing pyroxenites (Amundsen et al. 1987), then the preservation of the carbonates in the mantle xenoliths could have been possible only if they were formed by quenching of intruding carbonate melts shortly before the entrainment of the xenoliths in basaltic magma. In addition, isothermal decompression would result in decay of carbonates so that they may rarely survive their entrainment in host magmas from the mantle (Wyllie et al. 1983; Canil 1990). The majority of carbonate segregations in the Spitsbergen xenoliths show partial melting decomposition at the rims (Amundsen 1987; Ionov et al. 1993) and only in a few xenoliths have the primary carbonate assemblages been preserved.

Acknowledgements We wish to thank N.J. Pearson for help with electron microprobe analyses, W.L. Griffin and T.T. Win for guidance with proton probe analyses, D.M. Dashevskaya and A.N. Evdokimov for help in sample collection and processing. Comments and reviews of J. Dalton, D. Draper and an anonymous reviewer have been very helpful in improving the original version of the manuscript and are gratefully acknowledged. The study was supported by an ARC Research Fellowship to D.A. Ionov and ARC and Macquarie University research grants to S.Y. O'Reilly. This is Publication number 7 in the Key Centre for the Geochemical Evolution and Metallogeny of Continents (GEMOC).

References

Amundsen HEF (1987) Evidence for liquid immiscibility in the upper mantle. Nature 327:692–695

Amundsen HEF, Griffin WL, O'Reilly SY (1987) The lower crust and upper mantle beneath north-western Spitsbergen: evidence from xenoliths and geophysics. Tectonophysics 139:169–185

Brey GP, Green DH (1976) Solubility of CO_2 in olivine melilitite at high pressures and role of CO_2 in the Earth's upper mantle. Contrib Mineral Petrol 55:217–230

Brey GP, Köhler T (1990) Geothermobarometry in four-phase lherzolites. II. New thermo-barometers, and practical assessment of existing thermobarometers. J Petrol 31:1353–1378

Brey GP, Brice WR, Ellis DJ, Green DH, Harris KL, Ryabchikov ID (1983) Pyroxene-carbonate reactions in the upper mantle. Earth Planet Sci Lett 62:63–74

Bulanova GP, Pavlova LP (1987) Magnesite peridotite mineral association in a diamond from the Mir pipe. Trans Dokl Acad Sci Russ, Earth Sci Sect 295:176–179

Canil D (1990) Experimental study bearing on the absence of carbonate in mantle-derived xenoliths. Geology 18:1011–1013

Dalton JA, Wood BJ (1993a) The compositions of primary carbonate melts and their evolution through wallrock reaction in the mantle. Earth Planet Sci Lett 119:511–525

Dalton JA, Wood BJ (1993b) The partitioning of Fe and Mg between olivine and carbonate and the stability of carbonate under mantle conditions. Contrib Mineral Petrol 114:501–509

Dautria JM, Dupuy C, Takherist D, Dostal J (1992) Carbonate metasomatism in the lithospheric mantle: the peridotitic xenoliths from a melilititic district of the Sahara Basin. Contrib Mineral Petrol 111:37–52

Endress M, Bischoff A (1996) Carbonates in CI chondrites: clues to parent body evolution. Geochim Cosmochim Acta 60:489–507

Frezzotti M-L, Touret JLR, Lustenhouwer WJ, Neumann E-R (1994) Melt and fluid inclusions in dunite xenoliths from La Gomera, Canary Islands: tracking the mantle metasomatic fluids. Eur J Mineral 6:805–817

Frost BR (1985) On the stability of sulfides, oxides, and native metals in serpentinite. J Petrol 26:31–63

Furnes H, Pedersen RB, Maaloe S (1986) Petrology and geochemistry of spinel peridotite nodules and host basalt, Vestspitsbergen. Nor Geol Tidsskr 66:53–68

Galer SJG, O'Nions RK (1989) Chemical and isotopic studies of ultramafic inclusions from the San Carlos volcanic field, Arizona: a bearing on their petrogenesis. J Petrol 30:1033–1064

Genshaft YS, Ilupin IP (1987) Mineralogy of Quaternary volcanic rocks from Spitsbergen. Trans Dokl Acad Sci Russ, Earth Sci Sect 295:168–173

Genshaft YS, Dashevskaya DM, Yevdokimov AM, Kopylova MG (1992) Abundance and shape of plutonic ultramafic inclusions in alkalic basalt from Spitsbergen. Trans Dok Russ Acad Sci Russ, Earth Sci Sect 326: 116-122

Green DH, Hibberson W (1970) The instability of plagioclase in peridotite at high pressure. Lithos 3:209–221

Green DH, Wallace ME (1988) Mantle metasomatism by ephemeral carbonatite melts. Nature 336:459–462

Green TH, Adam J, Sie SH (1992) Trace element partitioning between silicate minerals and carbonatite at 25 kbar and application to mantle metasomatism. Mineral Petrol 46:179–184

Hauri EH, Shimizu N, Dieu JJ, Hart SR (1993) Evidence for hotspot-related carbonatite metasomatism in the oceanic upper mantle. Nature 365:221–227

Hofmann AW (1988) Chemical differentiation of the Earth: the relationship between mantle, continental crust, and oceanic crust. Earth Planet Sci Lett 90:297–314

Hunter RH, McKenzie D (1989) The equilibrium geometry of carbonate melts in rocks of mantle composition. Earth Planet Sci Lett 92:347–356

Ionov DA, Dupuy C, O'Reilly SY, Kopylova MG, Genshaft YS (1993) Carbonated peridotite xenoliths from Spitsbergen: implications for trace element signature of mantle carbonate metasomatism. Earth Planet Sci Lett 119:283–297

Ionov DA, Hofmann AW, Shimizu N (1994) Metasomatism-induced melting in mantle xenoliths from Mongolia. J Petrol 35:753–785

Ionov DA, O'Reilly SY, Ashchepkov IV (1995a) Feldspar-bearing lherzolite xenoliths in alkali basalts from Hamar-Daban, southern Baikal region, Russia. Contrib Mineral Petrol 122:174–190

Ionov DA, Prikhod'ko VS, O'Reilly SY (1995b) Peridotite xenoliths from the Sikhote-Alin, south-eastern Siberia, Russia: trace element signatures of mantle beneath a convergent continental margin. Chem Geol 120:275–294

Irving AJ, Wyllie PJ (1975) Subsolidus and melting relationships for calcite, magnesite and the join $CaCO_3$–$MgCO_3$ to 36 kbar. Geochim Cosmochim Acta 39:35–53

Jaques AL, Green DH (1980) Anhydrous melting of peridotite at 0–15 kbar pressure and the genesis of tholeiitic basalts. Contrib Mineral Petrol 73:287–310

Jones AP, Smith JS, Dawson JB, Hansen EC (1983) Metamorpjism, partial melting, and K-metasomatism of garnet-scapolite-kyanite granulite xenoliths from Lashaine, Tanzania. J Geol 91:143–165

Kogarko LN, Henderson CMB, Pacheco H (1995) Primary Ca-rich carbonatite magma and carbonate-silicate-sulphide liquid immiscibility in the upper mantle. Contrib Mineral Petrol 121:267–274

Lane SJ, Dalton JA (1994) Electron microprobe analysis of geological carbonates. Am Mineral 79:745–749

Macdonald R, Kjarsgaard BA, Skilling IP, Davies GR, Hamilton DL, Black S (1993) Liquid immiscibility between trachyte and carbonate in ash flow tuffs from Kenya. Contrib Mineral Petrol 114:276–287

McDonough WF (1990) Constraints on the composition of the continental lithospheric mantle. Earth Planet Sci Lett 101:1–18
McGetchin TR, Besancon JR (1973) Carbonate inclusions in mantle-derived pyropes. Earth Planet Sci Lett 18:408–410
Nickel KG, Green DH (1985) Empirical geothermobarometry for garnet peridotites and implications for the nature of the lithosphere, kimberlites and diamonds. Earth Planet Sci Lett 73:158–170
Olafsson M, Eggler DH (1983) Phase relations of amphibole, amphibole-carbonate, and phlogopite-carbonate peridotite: petrologic constraints on the asthenosphere. Earth Planet Sci Lett 64:305–315
O'Neill HSC (1981) The transition between spinel lherzolite and garnet lherzolite, and its use as a geobarometer. Contrib Mineral Petrol 77:185–194
O'Reilly SY, Griffin WL (1988) Mantle metasomatism beneath Victoria, Australia: I. Metasomatic processes in Cr-diopside lherzolites. Geochim Cosmochim Acta 52:433–447
Pouchou JL, Pichoir F (1984) A new model for quantitative X-ray microanalysis. 1. Application to the analysis of homogeneous samples. Rech Aerosp 5:13–38
Rudnick RL, McDonough WF, Chappell BC (1993) Carbonatite metasomatism in the northern Tanzanian mantle. Earth Planet Sci Lett 114:463–475
Ryabchikov ID, Brey G, Kogarko LN, Bulatov VK (1989) Partial melting of carbonatized peridotite at 50 kbar. Geochem Int 26:1–7
Ryan CG, Cousens DR, Sie SH, Griffin WL, Suter GF, Clayton E (1990) Quantitative PIXE microanalysis of geological materials using the CSIRO proton microprobe. Nucl Instrum Methods Phys Res B47:55–71
Sachtleben T, Seck HA (1981) Chemical control of Al-solubility in orthopyroxene and its implications on pyroxene geothermometry. Contrib Mineral Petrol 78:157–165
Schiano P, Clocchiatti R, Shimizu N, Weis D, Mattielli N (1994) Cogenetic silica-rich and carbonate-rich melts trapped in mantle minerals in Kerguelen ultramafic xenoliths: implications for metasomatism in the oceanic upper mantle. Earth Planet Sci Lett 123:167–178
Smith D (1987) Genesis of carbonate in pyrope from ultramafic diatremes on the Colorado Plateau, southwestern US. Contrib Mineral Petrol 97:389–396
Sweeney RJ, Prozesky V, Przybylowicz W (1995) Selected trace and minor element partitioning between peridotite minerals and carbonatite melts at 18–46 kbar pressure. Geochim Cosmochim Acta 59:3671–3683
Thibault Y, Edgar AD, Lloyd FE (1992) Experimental investigation of melts from a carbonated phlogopite lherzolite: implications for metasomatism in the continental lithospheric mantle. Am Mineral 77:784–794
Wallace ME, Green DH (1988) An experimental determination of primary carbonatite magma composition. Nature 335: 343–346
Wass SY (1979) Fractional crystallization in the mantle of late-stage kimberlitic liquids—evidence in xenoliths from the Kiama area, N.S.W., Australia. In: Boyd FR, Meyer HOA (Eds), The Mantle sample: inclusions in kimbarlites and other volcanics, Am Geohys Union, Washington, DC, pp 366–373
Wells PRA (1977) Pyroxene thermometry in simple and complex systems. Contrib Mineral Petrol 62:129–139
Witt-Eickschen G, Seck HA (1991) Solubility of Ca and Al in orthopyroxene from spinel peridotite: an improved version of an empirical geothermometer. Contrib Mineral Petrol 106: 431–439
Wyllie PJ (1987) Discussion of recent papers on carbonated peridotite, bearing on mantle metasomatism and magmatism. Earth Planet Sci Lett 82:391–:397
Wyllie PJ, Huang WL, Otto J, Byrnes AP (1983) Carbonation of peridotites and decarbonation of siliceous dolomites represented in the system $CaO–MgO–SiO_2–CO_2$ to 30 kbar. Tectonophysics 100:359–388
Yaxley GM, Crawford AJ, Green DH (1991) Evidence for carbonatite metasomatism in spinel peridotite xenoliths from western Victoria, Australia. Earth Planet Sci Lett 107:305–317
Zhang RY, Liou JG (1994) Significance of magnesite paragenesis in ultrahigh-pressure metamorphic rocks. Am Miner 79: 397–400